Voltage Tracking of Bidirectional DC-DC Converter Using Online Neural Network for Green Energy Application

Nor Farisha Diana [1*], Wahyu Mulyo Utomo [2], Afarulrazi Bin Abu Bakar [3], Suriana Salimin [4], Gigih Priyandoko [5], Widjonarko [6]
[1, 2, 3, 4] Department Electrical Engineering, Faculty of Electrical and Electronics Engineering, Universiti Tun Hussein Onn Malaysia, Johor, Malaysia
[5] Department of Electrical Engineering, Faculty of Engineering, Universitas Widyagama Malang, Indonesia
[6] Department of Electrical Engineering, Faculty of Engineering, Universitas Jember, Indonesia
Email: [1] farishadiana98@gmail.com, [2] wahyu@uthm.edu.my, [3] afarul@uthm.edu.my, [4] suriana@uthm.edu.my, [5] gigih@widyagama.ac.id, [6] widjonarko.teknik@unej.ac.id
*Corresponding Author

***Abstract*—In the current era, green energy systems like solar PV, wind energy, and battery storage critically rely on DC-DC converters to manage power flow and voltage conversion efficiently, ensuring optimal performance and reliability. Nevertheless, converters face multiple challenges, including efficiency losses, thermal management concerns, and electromagnetic interference, which can impact these green energy systems' overall performance and reliability. To overcome these challenges, it is necessary to utilize advanced control mechanisms, enhance heat management approaches, and optimize component design. Implementing these improvements will improve the effectiveness and durability of DC-DC converters in renewable energy applications. This research aims to analyze the performance characteristics of a three-phase interleaved half-bridge bidirectional (TPHB-Bi) converter. The research objective involves investigating the effectiveness of the proposed controller by rigorously assessing voltage tracking. This is done through comprehensive assessments of start-up procedures and reference voltage variations using MATLAB/Simulink. The study utilizes a neural network controller with an online learning algorithm based on backpropagation to enhance the converter's operational capabilities, ensuring a stable output voltage and improved transient response. The simulation results highlight the significant advantages of the proposed controller over a conventional PID controller. It exhibits a remarkable reduction in overshoot by 5.29%, considerably shorter rise times ranging from 0.01ms to 0.1ms, and faster settling times of 0.025s. The findings have great importance in promoting sustainable energy development and environmental protection. They demonstrate that implementing advanced control strategies for DC-DC converters can result in more efficient and reliable green energy systems.**

***Keywords*—Buck-Boost Converter; Interleaved Converter; Artificial Neural Network; Electric Vehicle.**

I. INTRODUCTION

The global shift towards renewable energy is gaining significance due to the adverse effects of fossil fuel utilization. Renewable energy sources such as wind, solar, and hydroelectric power provide a sustainable substitute for conventional fossil fuels [1]–[4]. The motivation behind this transition is the pressing necessity to decrease greenhouse gas emissions, address climate change, and minimize air pollution. Green energy significantly affects the transportation industry, specifically through the increasing popularity of electric vehicles (EVs) [5]–[9].

Electric vehicles are becoming increasingly popular as a vital environmentally friendly transportation solution. Unlike conventional automobiles powered by internal combustion engines (ICEVs), electric vehicles (EVs) do not emit any pollutants from their exhaust pipes, significantly reducing the overall carbon footprint [10]–[14]. Electric vehicles (EVs) have the potential to further improve their environmental benefits by utilizing the power that is generated from renewable sources, contributing to a future that is cleaner and more sustainable [15]–[20]. Many governments support the broad adoption of electric vehicles by implementing regulations and incentives designed to encourage environmentally responsible mobility. EVs are gaining attention for their eco-friendly nature, lower greenhouse gas (GHG) emissions, fuel costs, and reduced noise pollution. They generate ten times less CO2 than conventional internal combustion engine vehicles (ICEVs) [21]–[25]. Sustainable electric mobility is crucial to minimizing environmental harm and accelerating development. By 2040, most urban planning commissions worldwide aim to have transitioned their transportation networks to more environmentally friendly alternatives [26]–[28].

In EVs, DC-DC converters are essentially additional devices. They consist of power semiconductor devices that function as electrical switches, capable of handling large currents [29]–[33]. Consequently, the inductors used in these converters tend to be bulky, which reduces the overall power density of the devices. The filter inductor, input capacitor, and output capacitor also influence the size of the converter. Additionally, due to the switching process, DC-DC converters experience significant fluctuations in input current [34]–[38]. Interleaved or multi-phase techniques solve this problem [39][40]. An interleaved converter integrates multiple power stages operating in parallel. This configuration distributes the input current across different phases, providing several advantages. First, it increases the

converter's power capacity while reducing stress during switching operations. It also helps to reduce the fluctuation in inductor currents, leading to improved overall heat distribution within the converter [41]–[44] and could significantly reduce the current ripple and inductor peak current in the system [45][46]. Half-bridge bidirectional buck-boost DC-DC converters are popular due to their high demand in wind, solar, and energy storage systems. The converter design depends on the input supply voltage and the required output voltage in the system. Bidirectional DC-DC converters are designed to adjust voltage levels, allowing for both voltage increase (step-up) and decrease (step-down) [47]–[50]. These converters can transfer power in both directions and exhibit good dynamic response within the system [51]–[54]. The dynamic response needs to be improved in the converter because it helps maintain stable output voltage and current; also, a faster dynamic response can enhance the stability of the converter [55].

Several intelligent controllers have been explored to improve the dynamic response of bidirectional DC-DC converters, including fuzzy logic controllers, adaptive neuro-network controllers with hybrid PI-sliding methods, adaptive neuro-fuzzy inference systems, and model predictive controllers [56]–[60]. Implementing a fuzzy logic controller for a bidirectional DC-DC converter has been verified, demonstrating its ability to achieve smooth control in the system [61]. Ongoing research and development continuously improve these controllers, making them more suitable and significant for Evs [62][63]. As reported in [64]In recent years, new methods have emerged to enhance the effectiveness of bidirectional DC-DC converters. Neural network control (NNC) is another promising option due to its ability to update internal controller parameters, making it suitable for nonlinear systems. A buck converter has successfully demonstrated experimental verification of NNC for varying battery voltage [65][66]. NNC has also been applied in various other power electronics and drive applications [65][67][68]. To further improve NNC performance, research has focused on developing online learning schemes [69]–[72].

In order to design this system, several factors need to be considered. These include the number of switches that will be utilized, control stabilities of the output voltage, which are used to maintain the converter output voltage at the set point value, and set point determination, which is used to determine the set point voltage according to the type of load connection present in the system [73]–[75]. This research aims to describe an online learning neural network control (OL-NNC) for a three-phase interleaved half-bridge bidirectional DC-DC converter (TPHB-Bi). The development of the OL-NNC seeks to achieve the least steady-state error, overshoot, and output voltage rise time. It can learn instantly and adjust its controller parameters in response to external disturbances and internal variations of the converter.

The novelty of this research lies in developing and applying an OL-NNC for the TPHB-Bi converter, which aims to address the challenges of dynamic response and voltage regulation in bidirectional DC-DC converters. The OL-NNC is expected to improve performance metrics such as steady-state error, overshoot, and output voltage rise time. This study advances state-of-the-art power electronics for EV applications by providing a novel control strategy that leverages online learning capabilities to adapt to changing conditions and disturbances in real time.

This research involves designing, simulating, and analyzing the OL-NNC for the TPHB-Bi converter. The methodology includes the following steps: developing the neural network architecture, setting up simulations to test the performance of the OL-NNC under various operating conditions, and comparing it with traditional control methods. The key variables and parameters investigated include steady-state error, overshoot, rise time, and settling time.

This research makes the following significant contributions. The first aspect to consider is introducing and installing the OL-NNC, built explicitly for the TPHB-Bi converter. The OL-NNC can adapt and learn in real time, resulting in improved dynamic performance metrics of the converter, such as steady-state error, overshoot, and rise time. The TPHB-Bi converter exhibited enhanced dynamic response, characterized by decreased overshoot, accelerated rising time, and steady-state negligible mistake. The converter has been modified to provide stability and reliability, even when operating conditions change. It also has excellent voltage regulation capabilities, ensuring a stable output voltage throughout reference voltage changes and start-up procedures. Additionally, it performs better in managing voltage regulation in real-time applications. The proposed OL-NNC can be applied in green energy to enhance the efficiency and reliability of power management solutions for electric vehicles (EVs) and other renewable energy systems. It can be compared to traditional PID controllers, and its superior performance in various metrics can be highlighted. The effectiveness of the OL-NNC can be demonstrated through comprehensive simulation and validation, showing its ability to improve the performance of the TPHB-Bi converter in different scenarios.

The structure of the research paper is as follows: the second section discusses the operation modes of the TPHB-BI converter and also discusses the controller of the ANN using online learning methods, and the third section discusses the findings that have been simulated using MATLAB/Simulink for transient response during starting-up, dynamic response when voltage step-up and voltage step-down, impact of input voltage variations on the performance of the the-bi converter and comparison of the TPHB-Bi converter with OL-NNC and the PID. Finally, the structure of this paper is the conclusion, which summarizes the most critical issues and is presented in section 4.

II. METHOD

The method section explains the studied system and introduces the control structure for the converter. The first part of the method section provides a detailed explanation of the studied system, including the circuit diagram of the bidirectional converter and the symbols used in the analysis. The second part of this section describes the control structure of the neural network controller and online learning algorithm of backpropagation-based efficiency optimization control (BPEOC). A flowchart of the research methodology

is presented. The controller and BPEOC equations will be given step by step.

A. Model of a Bidirectional DC-DC Converter

The circuit diagram of the TPHB-Bi converter is shown in Fig. 1. The inductor, switch, and capacitor are the three main components of this converter. This converter's minimal number of elements achieves the simplicity of design and construction. The inductor is placed on the low-voltage side of the converter, and a capacitor can be connected in parallel with the load on both the high-voltage and low-voltage sites. It comprises three identical topological structures, each with two inputs labeled Vhigh and Vlow. MOSFETs are represented by S_1 to S_6, and their parasitic anti-parallel diodes are labeled D_{I1} to D_{I6}. Energy storage inductors are denoted as L_1 to L_3, and the load resistors and input/output filter capacitors are represented by R_1 to R_2 and C_1 to C_2, respectively. S_1, S_2, S_3, S_4, S_5, and S_6 are connected sequentially on a three-phase inverter bridge. The upper and lower power switches utilize a pulse-width modulation (PWM) phase-shift interleaved complementary control method, where the drive signal's phase angle differs by 120 degrees consecutively. The switching period T and the switching frequency of the system $fs = 1/T$ are defined.

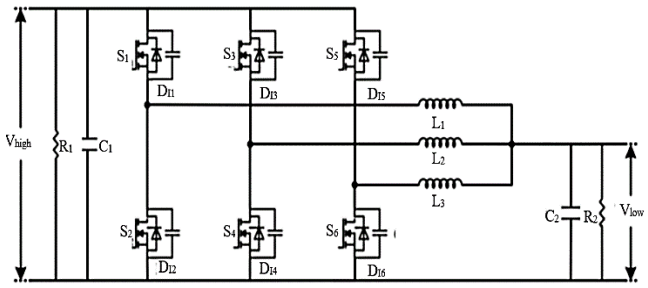

Fig. 1. Proposed TPHB-Bi Buck-Boost Converter

The mode of the TPHB-Bi converter is assumed to operate in continuous conduction mode (CCM), meaning six switches are conducting. Therefore, two operating modes are defined. In the first mode, switches S_1, S_3, and S_5 will, and S_2, S_4, and S_6 will open. In the second mode, switch S_2, S_4, and S6 will open, and switch S_1, S_3, and S_5 will open. Due to the similarities in operation, the explanation will focus on the boost mode [76][77]. The circuit's operation can be broken down into seven distinct stages. The operation stages of the TPBH-Bi converter are described as follows:

- Stage 1 - S_2, S_4, and S_6 are switched off simultaneously while D_{I1}, D_{I3}, and D_{I5} continue to conduct naturally. On the low voltage side, L_1, L_2, and L3 transmit electrical energy to the high voltage side.
- Stages 2 – S_2 turn on, S_4, and S_6 are switched off simultaneously while D_{I3}, and D_{I5} continue to conduct naturally and DI1 is off. On the low voltage side, the low voltage side, L_1, L_2, and L_3 transmit electrical energy to the high voltage side.
- Stages 3 – S_4 turn on, S_2, and S_6 are switched off simultaneously while D_{I1}, and D_{I5} continue to conduct naturally and DI3 is off. On the low voltage side, L_2, L_1, and L_3 transmit electrical energy to the high voltage side.
- Stages 4 – S_6 turn on, S_2, and S_4 are switched off simultaneously while D_{I1}, and D_{I3} continue to conduct naturally and D_{I5} is off. On the low voltage side, L_3, L_1, and L_2 transmit electrical energy to the high voltage side.
- Stages 5 – S_2 and S_4 turn on, S_6 are switched off simultaneously while D_{I5} continue to conduct naturally and D_{I1} and D_{I3} is off. On the low voltage side, L_1, L_2, and L_3 transmit electrical energy to the high voltage side.
- Stages 6 – S_2 and S_6 turn on, S_4 are switched off simultaneously while D_{I3} continue to conduct naturally and D_{I1} and D_{I5} is off. On the low voltage side, L_1, L_3, and L_2 transmit electrical energy to the high voltage side.
- Stages 7 – S_4 and S_6 turn on, S_2 are switched off simultaneously while D_{I1} continue to conduct naturally and D_{I3} and D_{I5} is off. On the low voltage side, L_2, L_3, and L_1 transmit electrical energy to the high voltage side.

The sequencing of the equivalent circuit depends on the duty cycle value. When the duty cycle of the switches is between 0 and 1/3, it follows a repeating sequence of stages 1-2-3-4. However, when the duty cycle exceeds 0.33, a new equivalent circuit emerges within the $1/3 < d \leq 2/3$ range. As a result, the sequences change to stages 6-2-5-3-7-4. As shown in Table I and Table II, the sequence of the operation of the MOSFET switch in seven stages has been discussed in buck and boost mode.

TABLE I. OPERATION STAGES IN BUCK MODE

Stages	Mosfet (ON)	Mosfet (OFF)
1		S_1, S_2, S_3, S_4, S_5, S_6
2	S_1	S_2, S_3, S_4, S_5, S_6
3	S_3	S_1, S_2, S_4, S_5, S_6
4	S_5	S_1, S_2, S_3, S_4, S_6
5	S_1, S_3	S_2, S_4, S_5, S_6
6	S_1, S_5	S_2, S_3, S_4, S_6
7	S_3, S_5	S_1, S_2, S_4, S_5

TABLE II. OPERATION STAGES IN BUCK MODE

Stages	Mosfet (ON)	Mosfet (OFF)
1		S_1, S_2, S_3, S_4, S_5, S_6
2	S_2	S_1, S_3, S_4, S_5, S_6
3	S_4	S_1, S_2, S_3, S_5, S_6
4	S_6	S_1, S_2, S_3, S_4, S_5
5	S_2, S_4	S_1, S_3, S_5, S_6
6	S_2, S_6	S_1, S_3, S_4, S_5
7	S_4, S_6	S_1, S_2, S_3, S_5

Fig. 2 and Fig. 3 show the fundamental waveforms of the PWM in the boost mode of the TPHB-Bi converter are presented when the duty cycle is between 0 to 1/3 and when the duty cycle from 1/3 to 2/3 for switches S2, S4, and S6.

B. Neural Structures and Learning Scheme

1) Design of Neural Network Controller

Information about the plant (system) is required to design the neural network control. The number of input and output neurons in each layer corresponds to the system's input and output signals, respectively. Fig. 4 illustrates the proposed neural network control of the TPHB-Bi Converter. Based on the number of neurons in each layer of the proposed neural network controller architecture, the network has a 2-3-1

neuron structure, meaning there are two neurons in the input layer, three neurons in the hidden layer, and one neuron in the output layer. The first input neuron receives the error signal, the difference between the desired and actual output signals. The second input neuron receives a signal that distinguishes between the error signals of the previous and current sampling times. Using this structure, the neural network controller is equipped to handle the essential inputs that influence the converter's performance while maintaining a manageable level of complexity [78]–[80]. This structure ensures the controller can reduce overshoot, minimize rise and settling times, and enhance overall system stability.

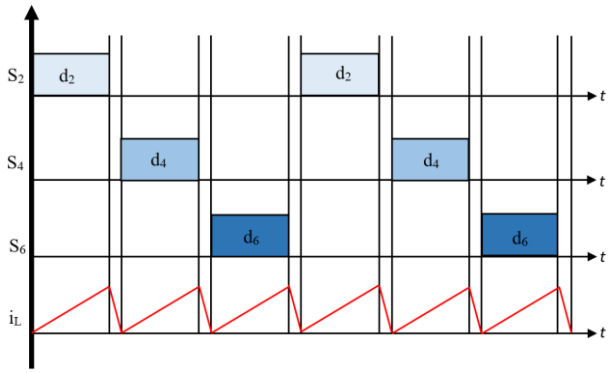

Fig. 2. PWM waveform of the proposed converter when the duty cycle is 0 < d ≤ 1/3

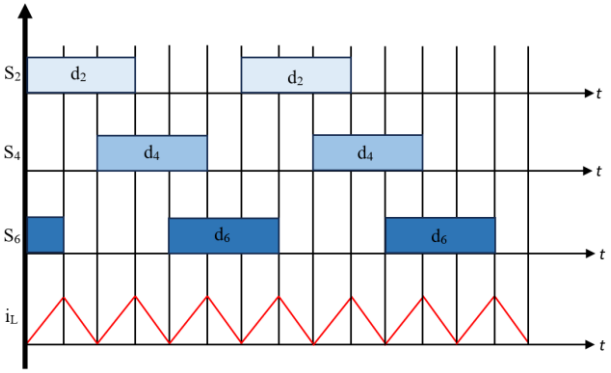

Fig. 3. PWM waveform of the proposed converter when the duty cycle is 1/3 < d ≤ 2/3

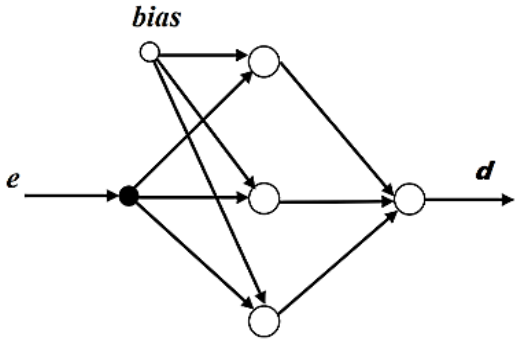

Fig. 4. The design of the neural network controller

W_{ij} represents the connection weight parameter between the j_{th} and i_{th} neurons in the m_{th} layer, and b_{mi} is the bias parameter of this layer in the i_{th} neuron. The network transfer function for the t_{th} neuron in the m_{th} layer is defined as (1).

$$n_i^m = \sum_{j=1}^{S^{m-1}} w_{ij}^m a_j^{m-1} + b_i^m \quad (1)$$

The neuron's m_{th} layer output function is provided by:

$$a_i^m a_i^m = f^m(n_i^m) \quad (2)$$

Where f is the neuron's activation function. The output layer and hidden layer in this design have activation functions of unity and a tangent hyperbolic function, respectively. The hidden layer's activation function is provided as.

$$f^m(n_i^m) = \frac{2}{1+e^{-2n_i^m}} - 1 \quad (3)$$

The connection weight and bias parameters are updated and provided by

$$w_{ij}^m(k+1) = w_{ij}^m(k) - \alpha \frac{\partial F(k)}{\partial w_{ij}^m} \quad (4)$$

$$b_i^m(k+1) = b_i^m(k) - \alpha \frac{\partial F(k)}{\partial b_i^m} \quad (5)$$

Where k is the sampling time, α is the learning rate, and F is the performance index function of the network.

2) Online Learning Algorithm of Backpropagation-Based Efficiency Optimization Control (BPEOC)

After the neural network architecture is modeled, the next stage defines the learning model to update network parameters. In general, sufficient training data for the input-output mapping of a plant is required in the learning mode of a neural network controller. The design of the learning algorithm for the learning process is then needed to update these parameters. In most cases, having ample training input-output mapping data of the plant is recommended to define network parameters. This mapping data enables the ANN controller to become familiar with the features of the plant and, hence, achieve accuracy in determining the control signal. The algorithm of the proposed online learning neural network as the efficiency optimization controller is as follows:

- Step 1- Initialization of network parameters, i.e., bias and weight.
- Step 2- Generate the input/output data table for distinct operating modes.
- Step 3- Randomly choose an input data pattern from the data table developed in Step 1, then compute its network output. The error pattern is derived based on the comparison of this calculated output and the desired output data.
- Step 4- From the derived error pattern, the network weight needs to be adjusted for updating by the backpropagation algorithm to achieve the slightest error.
- Step 5- The steps are repeated for each input-output data pattern set in the table until the error obtained for each set is satisfied for an acceptable error range.

- Step 6- Randomly test the network performance offline with various sets of the input pattern to ensure the network has successfully learnt the desired output pattern
- Step 7- After satisfactory learning, the weight and biases are downloaded for online testing.

The performance index used is the sum of squared errors, which is given by:

$$F(k) = \frac{1}{2}\sum_i e_i^2(k) \quad (6)$$

$$e_i(k) = t_i(k) - a_i(k) \quad (7)$$

where t_i is targeting signal and a_i output signal on last layer.

$$\frac{\partial F(k)}{\partial w_{ij}^m} = \frac{\partial F}{\partial n_i^m}\frac{\partial n_i^m}{\partial w_{ij}^m} \quad (8)$$

Defining the network's sensitivity parameter as below:

$$s_i^m = \frac{\partial F}{\partial n_i^m} \quad (9)$$

$$s_i^m = \frac{\partial F}{\partial a_i^m}\frac{\partial a_i^m}{\partial n_i^m} \quad (10)$$

The gradient between the connection weight parameter and the transfer function is provided by:

$$\frac{\partial a_i^m}{\partial n_i^m} = a_i^{m-1} \quad (11)$$

From substitution equation (9) and (11) into (4) the updating connection parameter is given by:

$$w_{ij}^{m-1}(k+1) = w_i^{m-i}(k) - \alpha s_i^m(k) a_i^{m-1}(k) \quad (12)$$

Using the identical method, the updating bias parameter is provided by:

$$b_i^m(k+1) = b_i^{m-1}(k) - \alpha s_i^m(k) \quad (13)$$

As a summary, Fig. 5 shows the flowchart of the research methodology. The steps performed are listed in order. The studied system consists of a converter and its control section.

III. Simulation and Discussion

The system consists of a TPHB-Bi converter and a controller. It is assumed that the reference value and system parameters are defined. The controller generates the duty cycle. This duty cycle needs to be transformed into a switching command signal, achievable through pulse width modulation. A comprehensive simulation was conducted to assess the stabilities of the controller performances in regulating the TPHB-Bi converter to utilize the performance. Simulink/MATLAB has been performed.

Fig. 6 shows a block diagram of the proposed OL-NNC control for a bidirectional DC-DC converter that operates in a closed-loop configuration. The model of the TPHB-Bi converter with the controller is shown in Fig. 7. The simulation parameters are shown in Table III.

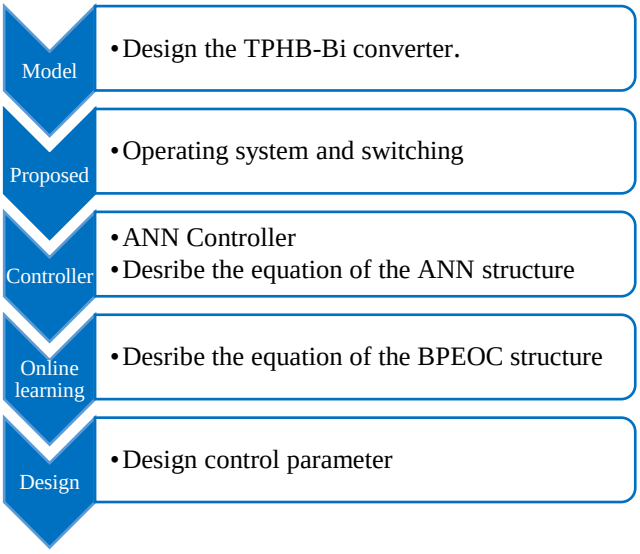

Fig. 5. Flowchart of the research methodology

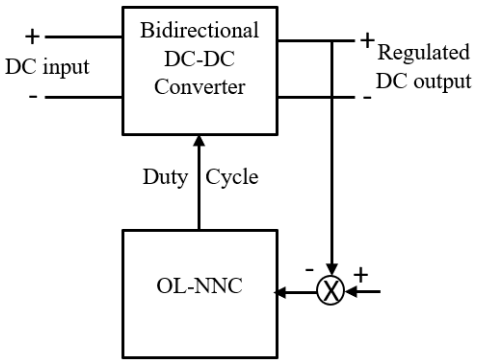

Fig. 6. Block diagram of the TPHB-Bi converter with controller

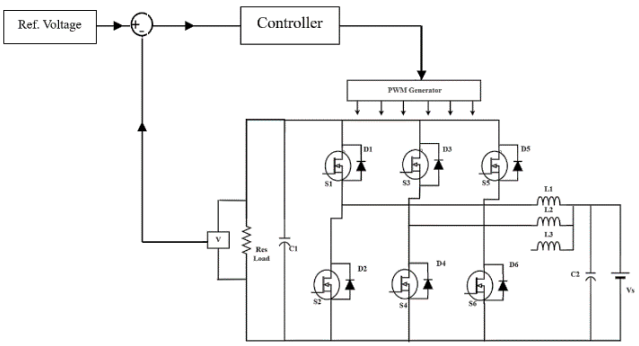

Fig. 7. Proposed model of the TPHB-Bi converter with proposed controller

TABLE III. Specification of the TPHB-Bi Converter

Parameters	Value	Unit
Input voltage	24	V
Voltage references	48,60	V
Inductor	250	µH
Capacitor	200	µF
Load resistor	100	Ω
Switching frequency	10	kHz

The performance of the system during start-up is presented in this section. Then, a comparison between the proposed control method and PID in the dynamic response

performance during step-up and step-down is investigated. The result shows the variation in the reference voltage of the output voltage. In this case, the step response for incremental changes is studied. The performance system under input voltage variation is investigated, and a discussion is presented.

A. Transient Response During Starting-up

Fig. 8 illustrates the result of the simulation of the output voltage of the TPHB-Bi converter when Vin is set to 24V during the simulation. With a reference voltage of 48V, the controller efficiently maintains and manages the output voltage to attain 48V. In this scenario, the duty cycle is approximated using the boost mode formula D = (Vref-Vin)/Vref, which is approximately equal to fifty percent. The output current can be determined by using the formula Io=Vo/R, which equals 0.48A. Since this is the case, the input current may be determined by applying the formula Iin = Io /(1 – D), which yields a value of 0.96 A. Within the context of this simulation, the conventional PID controller was contrasted with the OL-NNC that was presented.

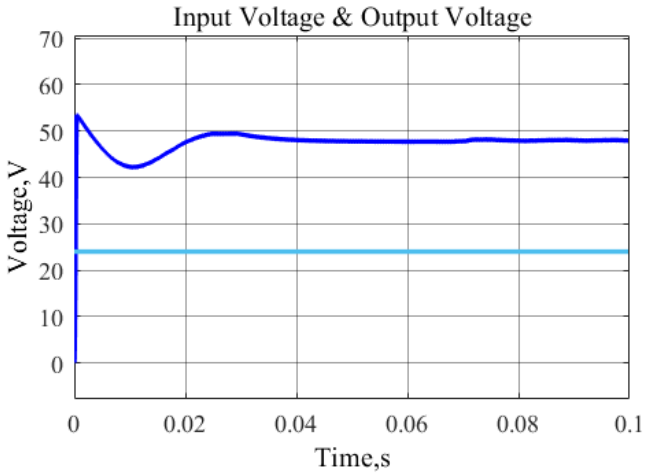

Fig. 8. Output voltage versus time waveform with Vin = 24V for OL-NNC controller

It has been discovered that the output voltage start-up transient responses utilizing OL-NNC in the TPHB-Bi converter with a reference voltage of 48V produce superior performances than the PID Controller. This is due to the fact that it eliminates overshoot and oscillation to reach the required output. Fig. 9 demonstrates that the settling time of an OL-NNC controller is approximately 0.045 seconds, significantly faster than the settling time of a PID controller, which is approximately 0.07 seconds. The percentage of overshoot for OL-NNC is also better than PID, as shown in Table IV. Table IV and Fig. 9 show that the OL-NNC controller has a better response than the PID controller.

TABLE IV. PERFORMANCE OF THE SYSTEM DURING START-UP

Parameter	PID	OL-NNC
Rise time, ms	0.368	0.335
Overshoot, V	55.92	53.38
Overshoot, %	16.5	11.21
Settling time, s	0.07	0.048

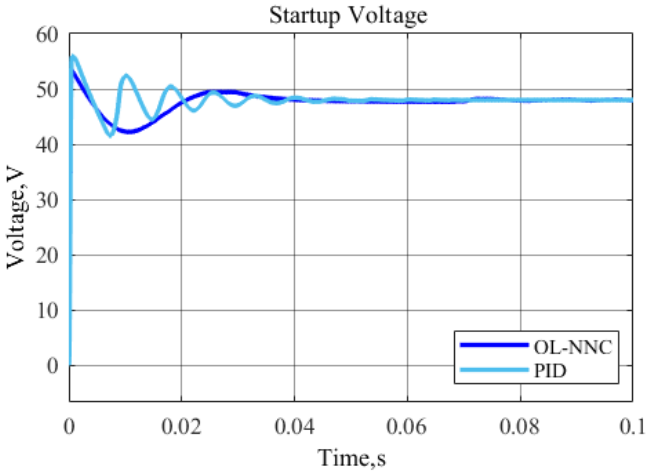

Fig. 9. Output voltage versus time waveform during start-up

B. Dynamic Response when Voltage Step-Up and Voltage Step-Down

Changes in the output reference voltage are examined in this section to evaluate the controller's performance. A step input can change the load resistance value at a desired time. Fig. 10 and Fig. 11 show the output voltage transient response of the TPHB-Bi converter to a reference voltage change. In Fig. 10, the reference voltage steps up from 48V to 60V. In this scenario, the OL-NNC performs significantly better than the PID controller. The OL-NNC achieves a lower overshoot voltage of 63.22V compared to the PID controller's 67.48V. Additionally, the OL-NNC controller reduces oscillation and has a faster settling time of around 0.02 seconds to reach stability in the system, compared to the PID controller. Table V summarizes the simulation performance during the voltage step-up.

TABLE V. PERFORMANCE OF THE SIMULATED CONTROLLER DURING VOLTAGE STEP UP

Parameter	PID	OL-NNC
Rise time, s	0.102	0.111
Overshoot, V	67.48	63.22
Overshoot, %	12.47	5.37
Settling time, s	0.18	0.15

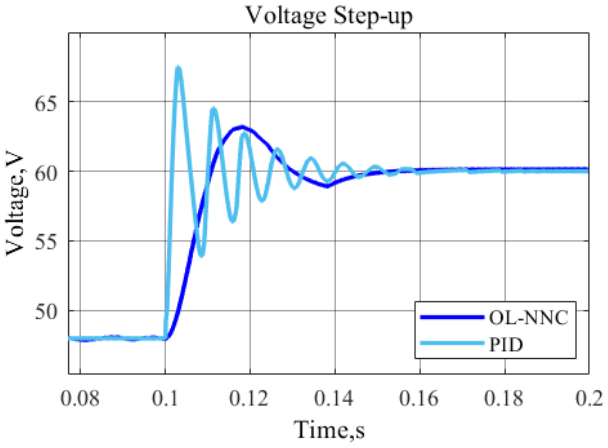

Fig. 10. Output voltage versus time waveform with references voltage step up from 48V to 60V

For reference, the voltage stepping down from 60V to 40V is shown in Fig. 11, and the undershoot of the PID controller is higher than that of the OL-NNC. Using the PID controller produces more oscillation and achieves stable performance. To achieve stability when the voltage references change in the system, the PID controller takes around 0.18s longer than the OL-NNC, which takes about 0.15s. Using the OL-NNC, the undershoot and oscillation have been reduced by around 7V compared to the PID controller, as shown in Table VI.

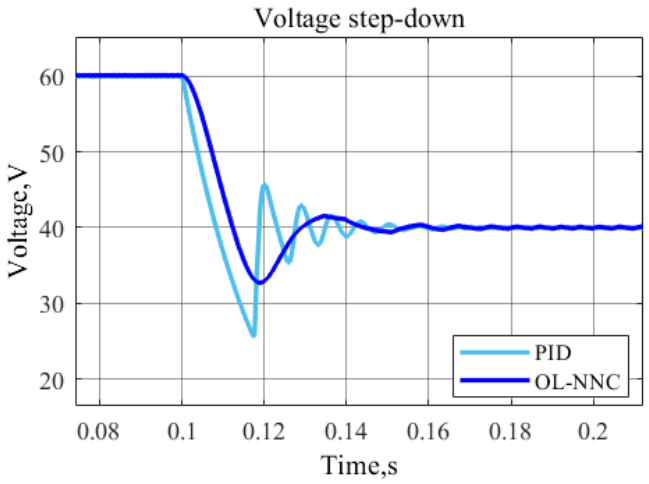

Fig. 11. Output voltage versus time waveform with references voltage step down from 60V to 40V

TABLE VI. PERFORMANCE OF THE SIMULATED CONTROLLER DURING VOLTAGE STEP DOWN

Parameter	PID	OL-NNC
Rise time, s	0.108	0.112
Overshoot, V	25.74	32.71
Overshoot, %	35.65	18.53
Settling time, s	0.18	0.15

C. *Impact of Input Voltage Variations on the Performance of the TPHB-Bi Converter*

The system's performance can be analyzed by examining its behavior in different operating settings. This section discusses the system's behavior when the input voltage changes from 24V to 36V. Fig. 12 presents the duty cycle produced by the OL-NNC controller when the input voltage changes from 24V to 30V at 0.2s using a step block. The duty cycle decreases when the input voltage increases in boost mode. To calculate the duty cycle, it needs to be multiplied by three due to the interleaved converter behavior.

Table VII presents the transient response data when the input voltage changes. Table VII presents data on the overshoot, rise time, and settling time for overshooting. When the value of the input voltage increases, the overshoot also increases, which is proportional to each other. For rise time, the lowest rise time is when the input voltage is at 36V, which is only 0.248ms, showing that this controller can respond quickly to fast input signals in the system. Lastly, for settling time, it is faster to achieve stability when the input voltage is increased, although the difference in values is minimal.

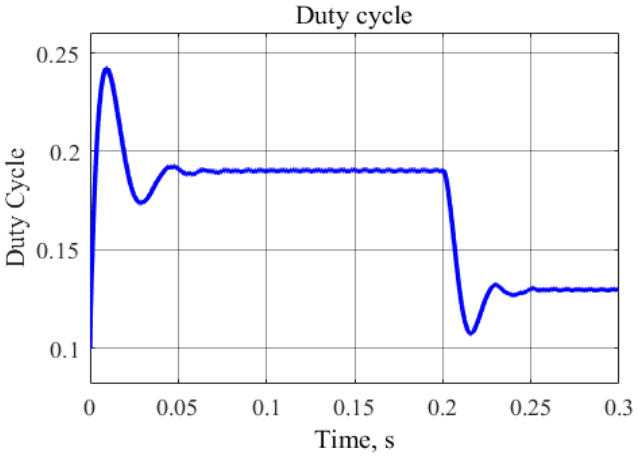

Fig. 12. Duty cycle produced by OL-NNC controller

TABLE VII. INPUT VOLTAGE VARIATIONS ON THE CONVERTER PERFORMANCE

Input voltage (V)	Transient Response		
	Overshoot (V)	Rise Time (ms)	Settling Time (s)
24	53.38	0.335	0.048
28	62.47	0.293	0.042
30	66.93	0.282	0.038
34	75.85	0.255	0.036
36	80.31	0.248	0.032

The summary in this section can be seen in Fig. 13, which shows the graph of these three components for transient response. The time axis can be referred to as rise time and settling time, while the voltage axis can be referred to as overshoot. It can be observed that the input voltage effectively tracks the performance of both the converter and controller.

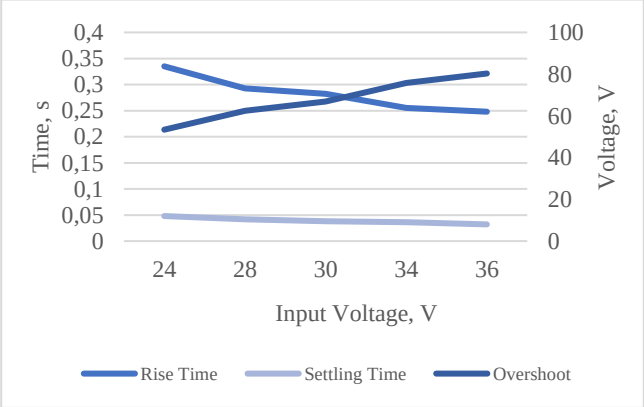

Fig. 13. Trend of the transient response of the TPHB-Bi converter with OL-NNC

D. *Comparison of the TPHB-Bi Converter with OL-NNC and the PID Approach*

In this section, a comparison is made between the OL-NNC controller method and the PID controller. Both controllers are designed to achieve the same stability for the system. The PID controller is configured with a designated operating point at a voltage reference of 48V and a load resistance of 100Ω. Notably, both systems are demonstrated with different output reference and input voltages.

Table VIII presents the values of overshoot voltage for various output voltage references. It is essential to highlight that the input voltage and the controlled bandwidth of the controller influence the overshoot voltage. Table VIII shows the overshoot for different reference voltages at different input voltages. The overshoot of the OL-NNC for every reference voltage at other input voltages is lower than that of the PID, which is suitable for the system as it is more stable. As shown in Fig. 14, a high overshoot can lead to system instability.

TABLE VIII. REFERENCE VOLTAGE VS OVERSHOOT IN DIFFERENCE INPUT VOLTAGE

Ref Voltage (V)	24V (V)		30V (V)		36V (V)	
	PID	*OL-NNC*	*PID*	*OL-NNC*	*PID*	*OL-NNC*
40	53.49	51.02	66.56	61.31	79.87	73.09
55	54.17	53.27	66.77	61.88	80.23	73.27
50	56.92	53.54	66.75	64.35	80.04	74.33
55	61.89	53.52	68.44	66.93	80.34	75.88
60	63.63	53.81	72.79	67.34	80.63	78.72

The overshoot of the OL-NNC for every reference voltage at different input voltages is lower than that of the PID, which is suitable for the system as it is more stable. As shown in Fig. 14, a high overshoot can lead to system instability.

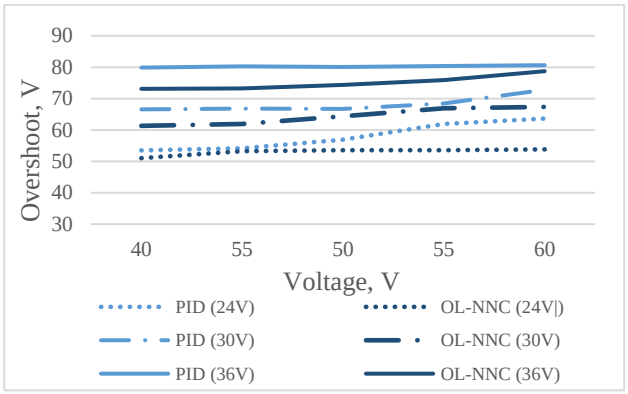

Fig. 14. Trend of overshoot vs. reference voltage in difference input voltage

Next, in Table IX, the rise time values are presented when the input voltage and output reference voltage change. Table IX shows the rise time in this system. For the OL-NNC, the rise time is slightly faster than the PID, ranging from around 0.001s to 0.01s, depending on the reference voltage and input voltage used in the system. The slowest rise time is for a 30V input voltage with the PID, around 0.389ms, and the fastest rise time is for the OL-NNC with a 36V input voltage, which is only 0.218ms.

TABLE IX. REFERENCE VOLTAGE VS RISE TIME IN DIFFERENCE INPUT VOLTAGE

Ref Voltage (V)	24V (ms)		30V (ms)		36V (ms)	
	PID	*OL-NNC*	*PID*	*OL-NNC*	*PID*	*OL-NNC*
40	0.339	0.308	0.257	0.252	0.219	0.218
55	0.359	0.339	0.296	0.282	0.240	0.251
50	0.384	0.355	0.351	0.304	0.265	0.256
55	0.389	0.386	0.368	0.324	0.274	0.288
60	0.381	0.367	0.374	0.364	0.310	0.305

Fig. 15 shows the rise time difference between the reference and input voltage graph. If the rise time takes longer to respond, a higher rise time can cause the output voltage to overshoot or undershoot its target value before settling. This can stress the components and reduce the overall stability of the system. However, using the OL-NNC controller has reduced the rise time. This reduction indicates a faster response to input voltage changes and changes in the reference voltage, enhancing the overall efficiency and stability of the converter.

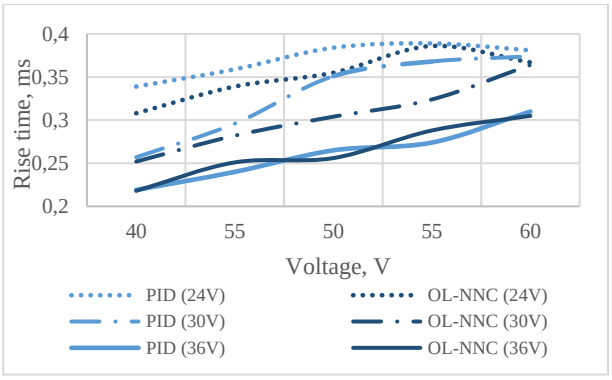

Fig. 15. Trend of rise time vs. reference voltage in difference input voltage

Lastly, for the settling time referring to an input voltage of 60V, it was the fastest steady state compared to the others. The lower settling time is for an input voltage of 24V at 40V, which takes around 0.071s to achieve a stable state. Table X shows that the OL-NNC achieves a stable state faster than the PID controller.

TABLE X. REFERENCE VOLTAGE VS SETTLING TIME IN DIFFERENCE INPUT VOLTAGE

Ref Voltage (V)	24V (s)		30V (s)		36V (s)	
	PID	*OL-NNC*	*PID*	*OL-NNC*	*PID*	*OL-NNC*
40	0.071	0.069	0.067	0.067	0.080	0.063
55	0.067	0.057	0.065	0.059	0.060	0.059
50	0.062	0.053	0.057	0.051	0.056	0.050
55	0.060	0.051	0.053	0.048	0.053	0.046
60	0.053	0.050	0.046	0.044	0.051	0.032

As shown in Fig. 16, the trends of the settling time indicate the difference between reference voltage and input voltage in this system. Implementing the OL-NNC has significantly enhanced the performance of the TPHB-Bi converter by ensuring a faster stabilization of the output, thereby improving the overall efficiency and stability of the converter. Additionally, using advanced algorithms in the OL-NNC ensures better damping of oscillations, leading to quicker stabilization.

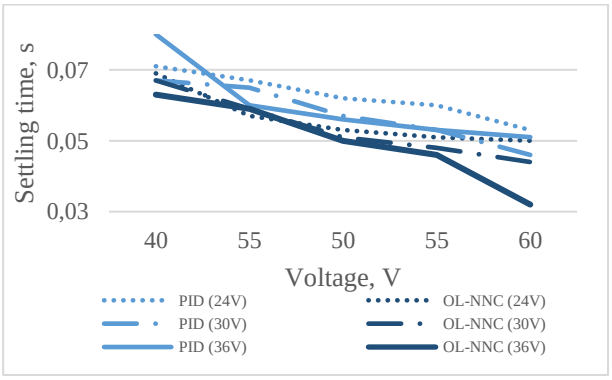

Fig. 16. Trend of settling time vs. reference voltage in difference input voltage

E. Strengths and Limitations

The performance analysis was performed using MATLAB/Simulink software, which demonstrated that the proposed neural network controller with an online learning algorithm significantly improves the dynamic response of the converter. This includes shorter rise times and faster settling times compared to PID controllers.

However, the neural network controller's design and implementation are more complex than conventional controllers. This includes sufficient training data and computational resources for real-time learning and adaptation. If not properly managed, the online learning algorithm could be overfitted to specific conditions, reducing its generalizability to different operating scenarios.

Although it can be said that this controller does not provide significant improvement, the OL-NNC controller can lead to stability and improve the control quality of the system. The output voltage, transient responsiveness, and dynamic properties cannot all be simultaneously improved using conventional PID control. It is evident that under step reference voltage variations, the proposed OL-NNC has better transient responses than those obtained from the PID controller.

IV. CONCLUSION

This paper discusses the application of an Artificial Neural Network (ANN) for the TPHB-Bi converter. An online learning technique based on the backpropagation scheme was used to improve the performance of the ANN controller. The designed ANN controller aims to regulate the output voltage of the TPHB-Bi converter. The simulation results demonstrate that implementing the OL-NNC technique is feasible for the TPHB-Bi converter. The outcomes indicate that the OL-NNC controller exhibits a faster response in tracking the desired output voltage, effectively reducing oscillations, overshoot, and settling time.

Future research will focus on optimizing the neural network architecture and exploring advanced techniques like deep learning to enhance controller efficiency and accuracy. Real-time hardware testing and validation are essential to evaluate performance under real-world conditions. Integrating the controller with other renewable energy sources and studying its application in microgrid environments will broaden its utility.

ACKNOWLEDGMENT

Communication of this research is made possible through monetary assistance from Universiti Tun Hussein Onn Malaysia and the UTHM Publisher's Office via Publication Fund E15216 and GPPS (Vot Q 301).

REFERENCES

[1] Q. Hassan *et al.*, "The renewable energy role in the global energy Transformations," *Renew. Energy Focus*, vol. 48, no. 100545, pp. 1–16, 2024, doi: 10.1016/j.ref.2024.100545.

[2] Q. Hassan, S. Algburi, A. Z. Sameen, H. M. Salman, and M. Jaszczur, "Green hydrogen: A pathway to a sustainable energy future," *Int. J. Hydrogen Energy*, vol. 50, pp. 310–333, 2024, doi: 10.1016/j.ijhydene.2023.08.321.

[3] L. S. Paraschiv and S. Paraschiv, "Contribution of renewable energy (hydro, wind, solar and biomass) to decarbonization and transformation of the electricity generation sector for sustainable development," *Energy Reports*, vol. 9, pp. 535–544, 2023, doi: 10.1016/j.egyr.2023.07.024.

[4] I. Kosmidis, D. Müller-Eie, and A. Delbosc, "Electric cars as a path to sustainable travel behaviour: Insights from Nord-Jæren," *Transp. Res. Part D Transp. Environ.*, vol. 125, pp. 1–14, 2023, doi: 10.1016/j.trd.2023.103982.

[5] J. Linn and V. McConnell, "Interactions between federal and state policies for reducing vehicle emissions," *Energy Policy*, vol. 126, pp. 507–517, 2019, doi: 10.1016/j.enpol.2018.10.052.

[6] A. M. Al-Ghaili, H. Kasim, H. Aris, and N. M. Al-Hada, "Can electric vehicles be an alternative for traditional fossil-fuel cars with the help of renewable energy sources towards energy sustainability achievement?," *Energy Informatics*, vol. 5, no. 4, pp. 1–24, 2022, doi: 10.1186/s42162-022-00234-3.

[7] D. Singh, U. K. Paul, and N. Pandey, "Does electric vehicle adoption (EVA) contribute to clean energy? Bibliometric insights and future research agenda," *Clean. Responsible Consum.*, vol. 8, p. 100099, 2023, doi: 10.1016/j.clrc.2022.100099.

[8] P. Albrechtowicz, "Electric vehicle impact on the environment in terms of the electric energy source — Case study," *Energy Reports*, vol. 9, pp. 3813–3821, 2023, doi: 10.1016/j.egyr.2023.02.088.

[9] F. Alanazi, "Electric Vehicles: Benefits, Challenges, and Potential Solutions for Widespread Adaptation," *Appl. Sci.*, vol. 13, no. 10, p. 6016, May 2023, doi: 10.3390/app13106016.

[10] A. A. Shalbaf, N. Shahidi, and M. Hemati, "A high-gain interleaved DC-DC converter with reduced components for EV charging application," *Comput. Electr. Eng.*, vol. 118, no. 109316, pp. 1–26, 2024, doi: 10.1016/j.compeleceng.2024.109316.

[11] J. A. Sanguesa, V. Torres-Sanz, P. Garrido, F. J. Martinez, and J. M. Marquez-Barja, "A Review on Electric Vehicles: Technologies and Challenges," *Smart Cities*, vol. 4, no. 1, pp. 372–404, Mar. 2021, doi: 10.3390/smartcities4010022.

[12] M. Guzek, J. Jackowski, R. S. Jurecki, E. M. Szumska, P. Zdanowicz, and M. Żmuda, "Electric Vehicles—An Overview of Current Issues—Part 1—Environmental Impact, Source of Energy, Recycling, and Second Life of Battery," *Energies*, vol. 17, no. 1, p. 249, Jan. 2024, doi: 10.3390/en17010249.

[13] I. Veza, M. Z. Asy'ari, M. Idris, V. Epin, I. M. Rizwanul Fattah, and M. Spraggon, "Electric vehicle (EV) and driving towards sustainability: Comparison between EV, HEV, PHEV, and ICE vehicles to achieve net zero emissions by 2050 from EV," *Alexandria Eng. J.*, vol. 82, pp. 459–467, 2023, doi: 10.1016/j.aej.2023.10.020.

[14] X. Zhao, H. Hu, H. Yuan, and X. Chu, "How does adopting electric vehicles reduce carbon emissions? Evidence from China," *Heliyon*, vol. 9, no. 9, pp. 1–13, 2023, doi: 10.1016/j.heliyon.2023.e20296.

[15] J. Gupta, R. Maurya, and S. R. Arya, "Designing an On-board Charger to Charge Multiple Electric Vehicles Efficiently," *Chinese J. Electr. Eng.*, vol. 9, no. 2, pp. 38–56, 2023, doi: 10.23919/CJEE.2023.000019.

[16] F. Wang, Y. Wang, B. Su, and C. Teng, "Three-phase interleaved high step-up bidirectional DC-DC converter," *IET Power Electron.*, vol. 13, no. 12, pp. 2638–2650, 2020, doi: 10.1049/iet-pel.2020.0295.

[17] S. C. Devi, A. Ramkumar, and S. Rajendran, "Design and Analysis of Three Stage Interleaved Boost Converter for E-Vehicle Application," vol. 6, no. 3, pp. 3666–3670, 2021.

[18] Y. Huang *et al.*, "Bidirectional Buck-Boost and Series LC-Based Power Balancing Units for Photovoltaic DC Collection System," *IEEE J. Emerg. Sel. Top. Power Electron.*, vol. 9, no. 6, pp. 6726–6738, 2021, doi: 10.1109/JESTPE.2021.3074575.

[19] Y. Wang, Y. Li, Y. Guan, and D. Xu, "Topology and Control Optimization of Bidirectional DC/DC Converter for Electric Vehicles," *IEEE J. Emerg. Sel. Top. Power Electron.*, vol. 12, no. 1, pp. 257–268, 2024, doi: 10.1109/JESTPE.2023.3278718.

[20] M. Rezvanyvardom and A. Mirzaei, "Zero-Voltage Transition Nonisolated Bidirectional Buck-Boost DC-DC Converter with Coupled Inductors," *IEEE J. Emerg. Sel. Top. Power Electron.*, vol. 9, no. 3, pp. 3266–3275, 2021, doi: 10.1109/JESTPE.2020.2992007.

[21] Z. Gholami, R. Ildarabadi, H. Heydari-Doostabad, M. Monfared, and T. O'Donnell, "Bidirectional wide range and high voltage gain buck-boost DC-DC converter for EV chargers empowering V2G-G2V applications," *IET Power Electron.*, vol. 17, no. 2, pp. 230–250, 2024, doi: 10.1049/pel2.12630.

[22] Y. G. Oh, O. Kwon, and J. M. Kwon, "Bidirectional push–pull/H-bridge converter for low-voltage energy storage system," *IET Power Electron.*, vol. 17, no. 1, pp. 1–9, 2024, doi: 10.1049/pel2.12586.

[23] E. Martinez-Vera and P. Bañuelos-Sanchez, "Review of Bidirectional DC-DC Converters and Trends in Control Techniques for Applications in Electric Vehicles," *IEEE Lat. Am. Trans.*, vol. 22, no. 2, pp. 144–155, 2024, doi: 10.1109/TLA.2024.10412031.

[24] A. Zabetian-Hosseini, G. Joos, and B. Boulet, "Control Design for Effective Usage of Electric Vehicles in V2G-Enabled DC Charging Stations," *IEEE Trans. Power Deliv.*, vol. 38, no. 6, pp. 4335–4346, 2023, doi: 10.1109/TPWRD.2023.3317804.

[25] Y. Li, Y. Wang, Y. Guan, and D. Xu, "Design and Analysis of Integrated Bidirectional DC-DC Converter for Energy Storage Systems," *IEEE Trans. Ind. Electron.*, pp. 1–12, 2023, doi: 10.1109/TIE.2023.3340186.

[26] G. Hill, O. Heidrich, F. Creutzig, and P. Blythe, "The role of electric vehicles in near-term mitigation pathways and achieving the UK' s carbon budget," *Appl. Energy*, vol. 251, p. 113111, 2019, doi: 10.1016/j.apenergy.2019.04.107.

[27] A. Dik, S. Omer, and R. Boukhanouf, "Electric vehicles : V2G for rapid, safe, and green EV penetration," *Energies 2022*, vol. 15, no. 803, 2022, doi: 10.3390/en15030803.

[28] Z. Yan *et al.*, "Ripple-Free Bidirectional DC-DC Converter With Wide ZVS Range for Battery Charging/Discharging System," *IEEE Trans. Ind. Electron.*, vol. 70, no. 10, pp. 9992–10002, 2023, doi: 10.1109/TIE.2022.3222659.

[29] M. N. Huynh, H. N. Duong, and V. H. Nguyen, "A Passivity-based Control Combined with Sliding Mode Control for a DC-DC Boost Power Converter," *J. Robot. Control*, vol. 4, no. 6, pp. 780–790, 2023, doi: 10.18196/jrc.v4i6.20071.

[30] O. O. Babayomi, Z. Zhang, Z. Li, and K. B. Park, "Bidirectional DC-DC converters for distributed energy resources: Robust predictive control with structurally-adaptive extended state observers," *Int. J. Electr. Power Energy Syst.*, vol. 158, 2024, doi: 10.1016/j.ijepes.2024.109913.

[31] M. Zhu, X. Liu, and X. Pan, "Design and implementation of real-time simulation module for non-isolated bidirectional half-bridge DC–DC converter," *Energy Reports*, vol. 8, pp. 15531–15547, 2022, doi: 10.1016/j.egyr.2022.11.148.

[32] R. D. N. Aditama, N. Ramadhani, T. Ardriani, J. Furqani, A. Rizqiawan, and P. A. Dahono, "New Modular Multilevel DC–DC Converter Derived from Modified Buck–Boost DC–DC Converter," *Energies*, vol. 16, no. 19, 2023, doi: 10.3390/en16196950.

[33] M. Afkar, R. Gavagsaz-Ghoachani, M. Phattanasak, S. Pierfederici, and W. Saksiri, "Local-Stability Analysis of Cascaded Control for a Switching Power Converter," *J. Robot. Control*, vol. 5, no. 1, pp. 160–172, 2024, doi: 10.18196/jrc.v5i1.20302.

[34] D. H. Al-Mamoori, N. A. Azli, S. M. Ayob, and A. A. A. Albakry, "A multilevel boost inverter with removed leakage current and a reduced number of elements for photovoltaic applications," *Int. J. Power Electron. Drive Syst.*, vol. 15, no. 1, pp. 312–322, 2024, doi: 10.11591/ijpeds.v15.i1.pp312-322.

[35] D. Maheswaran, S. V. Thazhathu, and D. Thangavelusamy, "A non-inverting single-switch buck-boost converter based LED driver," *Int. J. Power Electron. Drive Syst.*, vol. 14, no. 3, pp. 1509–1522, 2023, doi: 10.11591/ijpeds.v14.i3.pp1509-1522.

[36] W. Abitha Memala, C. Bhuvaneswari, S. M. Shyni, G. Merlin Sheeba, M. S. Mahendra, and V. Jaishree, "DC-DC converter based power management for go green applications," *Int. J. Power Electron. Drive Syst.*, vol. 10, no. 4, pp. 2046–2054, 2019, doi: 10.11591/ijpeds.v10.i4.pp2046-2054.

[37] M. A. N. Amran, A. A. Bakar, M. H. A. Jalil, A. F. H. A. Gani, and E. Pathan, "Optimal tuning of proportional-integral controller using system identification for two-phase boost converter for low-voltage applications," *Int. J. Power Electron. Drive Syst.*, vol. 12, no. 4, pp. 2393–2402, 2021, doi: 10.11591/ijpeds.v12.i4.pp2393-2402.

[38] M. C. Annamalai and N. Amutha prabha, "A comprehensive review on isolated and non-isolated converter configuration and fast charging technology: For battery and plug in hybrid electric vehicle," *Heliyon*, vol. 9, no. 8, p. e18808, 2023, doi: 10.1016/j.heliyon.2023.e18808.

[39] M. Hassanifar, D. Nazarpour, S. Golshannavaz, and Y. Neyshabouri, "A Modular Cascaded Multilevel Converter With High Configurability: Design, Analysis, and Optimization Study," *IEEE J. Emerg. Sel. Top. Power Electron.*, vol. 11, no. 1, pp. 850–861, 2023, doi: 10.1109/JESTPE.2021.3114501.

[40] W. C. Leal, M. O. Godinho, R. F. Bastos, C. R. De Aguiar, G. H. F. Fuzato, and R. Q. MacHado, "Cascaded Interleaved DC-DC Converter for a Bidirectional Electric Vehicle Charging Station," *IEEE Trans. Ind. Electron.*, vol. 71, no. 4, pp. 3708–3717, 2024, doi: 10.1109/TIE.2023.3273281.

[41] A. A. M. Faudzi, S. F. Toha, R. A. Hanifah, N. F. Hasbullah, and N. A. Kamisan, "An interleaved DC charging solar system for electric vehicle," *Int. J. Power Electron. Drive Syst.*, vol. 12, no. 4, pp. 2414–2422, 2021, doi: 10.11591/ijpeds.v12.i4.pp2414-2422.

[42] S. Farhani, A. N'Diaye, A. Djerdir, and F. Bacha, "Design and practical study of three-phase interleaved boost converter for fuel cell electric vehicle," *J. Power Sources*, vol. 479, p. 228815, 2020, doi: 10.1016/j.jpowsour.2020.228815.

[43] R. R. de Melo, F. L. Toffoli, S. Daher, and F. L. M. Antunes, "Interleaved bidirectional DC-DC converter for electric vehicle applications based on multiple energy storage devices," Electron. *Eng.*, vol. 102, no. 4, pp. 2011–2023, 2020, doi: 10.1007/s00202-020-01009-3.

[44] P. Purna Chandra Rao, R. Anandhakumar, and L. Shanmukha Rao, "Analysis of a novel soft switching bidirectional DC-DC converter for electric vehicle," *Bull. Electr. Eng. Informatics*, vol. 12, no. 5, pp. 2665–2672, 2023, doi: 10.11591/eei.v12i5.4505.

[45] Y. E. Wu and W. C. Huang, "Dual-Input Interleaved Bidirectional DC-DC Converter for Light Electric Vehicles," *IEEE J. Emerg. Sel. Top. Power Electron.*, vol. 11, no. 5, pp. 5037–5051, 2023, doi: 10.1109/JESTPE.2023.3294231.

[46] O. Asvadi-Kermani, B. Felegari, H. Momeni, S. Alireza Davari, and J. Rodriguez, "Dynamic Neural-Based Model Predictive Voltage Controller for an Interleaved Boost Converter With Adaptive Constraint Tuning," *IEEE Trans. Ind. Electron.*, vol. 70, no. 12, pp. 12739–12751, 2023, doi: 10.1109/TIE.2023.3234138.

[47] P. Abolhassani, M. Maalandish, A. Nadermohammadi, M. B. B. Sharifian, M. R. Feyzi, and S. H. Hosseini, "A high step-up high step-down coupled inductor based bidirectional DC-DC converter with low voltage stress on switches," *IET Power Electron.*, pp. 1–22, 2024, doi: 10.1049/pel2.12694.

[48] K. Farajzadeh, L. Mohammadian, S. Shahmohammadi, and T. Abedinzadeh, "A novel bidirectional DC-DC converter with high voltage conversion ratio and capability of canceling input current ripple," *IET Power Electron.*, vol. 17, no. 3, pp. 375–393, 2024, doi: 10.1049/pel2.12649.

[49] X. Cui and A. T. Avestruz, "Large-Signal Stability Guarantees for Cycle-by-Cycle Controlled DC-DC Converters," *IEEE Control Syst. Lett.*, vol. 7, no. 3, pp. 763–768, 2023, doi: 10.1109/LCSYS.2022.3225586.

[50] R. Pramanik and B. B. Pati, "Modelling and controlling a non-isolated half-bridge bidirectional DC-DC converter with an energy management topology applicable with EV/HEV," *J. King Saud Univ. - Eng. Sci.*, vol. 35, no. 2, pp. 116–122, 2023, doi: 10.1016/j.jksues.2021.03.004.

[51] M. D. Keshavarzi and M. H. Ali, "A novel bidirectional dc-dc converter for dynamic performance enhancement of hybrid ac/dc microgrid," *Electron.*, vol. 9, no. 10, pp. 1–20, 2020, doi: 10.3390/electronics9101653.

[52] S. Wijanarko, G. I. Hasyim, J. Furqani, A. Rizqiawan, P. A. Dahono, and A. Muqorobin, "A bidirectional power converter connecting electric vehicle battery and DC microgrid," *Int. J. Power Electron. Drive Syst.*, vol. 15, no. 2, p. 978, 2024, doi: 10.11591/ijpeds.v15.i2.pp978-992.

[53] Y. Li, B. Zhao, J. Wan, Z. Yang, F. Liu, and M. Shahidehpour, "A Multiobjective Adaptive Switching Control for Bidirectional DC/DC Converter," *IEEE J. Emerg. Sel. Top. Power Electron.*, vol. 12, no. 2, pp. 1619–1628, 2024, doi: 10.1109/JESTPE.2023.3337944.

[54] N. A. Madiseh, E. Adib, and M. R. Amini, "A Novel Soft Switching Non-Isolated Bidirectional dc-dc Converter Without Any Extra Auxiliary Switch," *IEEE J. Emerg. Sel. Top. Power Electron.*, vol. 12, no. 2, pp. 1875–1882, 2024, doi: 10.1109/JESTPE.2023.3250435.

[55] H. J. Choi, K. W. Heo, and J. H. Jung, "A Hybrid Switching Modulation of Isolated Bidirectional DC-DC Converter for Energy

Storage System in DC Microgrid," *IEEE Access*, vol. 10, pp. 6555–6568, 2022, doi: 10.1109/ACCESS.2021.3138988.

[56] C. S. Purohit, M. Geetha, P. Sanjeevikumar, P. K. Maroti, S. Swami, and V. K. Ramachandaramurthy, "Performance analysis of DC/DC bidirectional converter with sliding mode and pi controller," *Int. J. Power Electron. Drive Syst.*, vol. 10, no. 1, pp. 357–365, 2019, doi: 10.11591/ijpeds.v10.i1.pp357-365.

[57] W. I. Hameed, B. A. Sawadi, and A. M. Fadhil, "Voltage tracking control of DC-DC boost converter using fuzzy neural network," *Int. J. Power Electron. Drive Syst.*, vol. 9, no. 4, pp. 1657–1665, 2018, doi: 10.11591/ijpeds.v9.i4.pp1657-1665.

[58] O. Y. Her, M. S. A. Mahmud, M. S. Z. Abidin, R. Ayop, and S. Buyamin, "Artificial neural network based short term electrical load forecasting," *Int. J. Power Electron. Drive Syst.*, vol. 13, no. 1, pp. 586–593, 2022, doi: 10.11591/ijpeds.v13.i1.pp586-593.

[59] S. Burada and K. Padma, "Model predictive current control for maximum power point tracking of voltage source inverter based grid-connected photovoltaic system," *Int. J. Power Electron. Drive Syst.*, vol. 14, no. 3, pp. 1781–1790, 2023, doi: 10.11591/ijpeds.v14.i3.pp1781-1790.

[60] T. Randjaka, S. J. Rajonirina, F. P. Andriniriniaimalaza, and J. N. Razafinjaka, "An ANFIS Control Approach of a Bi-Directional Buck-Boost used for a Battery," *Int. J. Eng. Manag. Res.*, vol. 12, no. 3, pp. 30–39, 2022, doi: 10.31033/ijemr.12.3.5.

[61] I. Journal and M. Trends, "Fuzzy Logic Based a Bidirectional DC/DC Converter with Dual-Battery Energy Storage for Hybrid Electric Vehicle System," *Int. J. Mod. Trends Sci. Technol.*, vol. 5, pp. 133–137, 2019.

[62] Y. Wang, Y. Wang, X. Song, and Z. Liang, "Finite-Time Adaptive Neural Network Observer-Based Output Voltage-Tracking Control for DC-DC Boost Converters," *IEEE Trans. Circuits Syst. I Regul. Pap.*, vol. 70, no. 7, pp. 3005–3016, 2023, doi: 10.1109/TCSI.2023.3264536.

[63] C. P. Ragasudha and S. Hemamalini, "Performance Analysis of a High Gain Bidirectional DC-DC Converter Fed Drive for an Electric Vehicle With Battery Charging Capability During Braking," *IEEE Access*, vol. 12, pp. 14499–14511, 2024, doi 10.1109/ACCESS.2024.3357726.

[64] T. Sutikno, "Application of non-isolated bidirectional DC-DC converters for renewable and sustainable energy systems : a review," *Clean Energy*, vol. 7, no. 2, pp. 293–311, 2023, doi: https://doi.org/10.1093/ce/zkac070.

[65] W. Dong, S. Li, X. Fu, Z. Li, M. Fairbank, and Y. Gao, "Control of a Buck DC/DC Converter Using Approximate Dynamic Programming and Artificial Neural Networks," *IEEE Trans. Circuits Syst. I Regul. Pap.*, vol. 68, no. 4, pp. 1760–1768, 2021, doi: 10.1109/TCSI.2021.3053468.

[66] X. Cui and A. T. Avestruz, "Fast-Response Variable Frequency DC-DC Converters Using Switching Cycle Event-Driven Digital Control," *IEEE Trans. Power Electron.*, vol. 38, no. 7, pp. 8190–8207, 2023, doi: 10.1109/TPEL.2023.3263516.

[67] S. Arandhakar, N. Jayaram, Y. R. Shankar, Gaurav, P. S. V. Kishore, and S. Halder, "Emerging Intelligent Bidirectional Charging Strategy Based on Recurrent Neural Network Accosting EMI and Temperature Effects for Electric Vehicle," *IEEE Access*, vol. 10, pp. 121741–121761, 2022, doi 10.1109/ACCESS.2022.3223443.

[68] M. Gheisarnejad and M. H. Khooban, "IoT-Based DC/DC Deep Learning Power Converter Control: Real-Time Implementation," *IEEE Trans. Power Electron.*, vol. 35, no. 12, pp. 13621–13630, 2020, doi: 10.1109/TPEL.2020.2993635.

[69] V. Govindan and N. Pappa, "Online learning based neural network adaptive controller for efficient power tracking of PWR type reactor with unknown internal dynamics," *Ann. Nucl. Energy*, vol. 168, p. 108866, 2022, doi: 10.1016/j.anucene.2021.108866.

[70] E. Kalaiyarasan and S. Singaravelu, "Design and Performance Analysis of Bi-Directional DC-DC Buck/Boost Converter for Energy Storage Systems Using Advanced Control Strategies," *SSRG Int. J. Electron. Commun. Eng.*, vol. 11, no. 3, pp. 53–62, 2024, doi: 10.14445/23488549/IJECE-V11I3P106.

[71] S. K. Ramu, I. Vairavasundaram, B. Palaniyappan, A. Bragadeshwaran, and B. Aljafari, "Enhanced energy management of DC microgrid: Artificial neural networks-driven hybrid energy storage system with integration of bidirectional DC-DC converter," *J. Energy Storage*, vol. 88, p. 111562, 2024, doi: 10.1016/j.est.2024.111562.

[72] A. A. Mutlag, M. Kdair Abd, and S. W. Shneen, "Power Management and Voltage Regulation in DC Microgrid with Solar Panels and Battery Storage System," *J. Robot. Control*, vol. 5, no. 2, pp. 397–407, 2024, doi: 10.18196/jrc.v5i2.20581.

[73] M. R. Banaei, M. Golmohamadi, and H. Afsharirad, "A bidirectional high voltage ratio DC-DC topology for energy storage systems in a microgrid," *IET Power Electron.*, vol. 17, no. 2, pp. 281–294, 2024, doi: 10.1049/pel2.12637.

[74] I. Sudiharto, F. D. Murdianto, and A. Wulandari, "Adaptive charging control using ANN-PID controllers on multiple DC loads with varying battery voltages," *Int. J. Power Electron. Drive Syst.*, vol. 13, no. 1, pp. 620–630, 2022, doi: 10.11591/ijpeds.v13.i1.pp620-630.

[75] Z. Fu, Y. Wang, F. Tao, and P. Si, "An adaptive nonsingular terminal sliding mode control for bidirectional dc-dc converter in hybrid energy storage systems," *Can. J. Electr. Comput. Eng.*, vol. 43, no. 4, pp. 282–289, 2020, doi: 10.1109/CJECE.2020.2972576.

[76] C. Zhang, B. Xu, J. Jasni, M. A. M. Radzi, N. Azis, and Q. Zhang, "Model Control and Digital Implementation of the Three Phase Interleaved Parallel Bidirectional Buck-Boost Converter for New Energy Electric Vehicles," *Energies*, vol. 15, no. 19, 2022, doi: 10.3390/en15197178.

[77] A. Mansouri, R. Gavagsaz-Ghoachani, M. Phattanasak, and S. Pierfederici, "Nonlinear Cascaded Control for a DC-DC Boost Converter," *J. Robot. Control*, vol. 4, no. 4, pp. 521–536, 2023, doi: 10.18196/jrc.v4i4.18932.

[78] C. L. Kuo, E. E. Kuruoglu, and W. K. V. Chan, "Neural Network Structure Optimization by Simulated Annealing," *Entropy*, vol. 24, no. 3, pp. 1–18, 2022, doi: 10.3390/e24030348.

[79] Y. Chu, J. Fei, and S. Hou, "Adaptive Global Sliding-Mode Control for Dynamic Systems Using Double Hidden Layer Recurrent Neural Network Structure," *IEEE Trans. Neural Networks Learn. Syst.*, vol. 31, no. 4, pp. 1297–1309, 2020, doi: 10.1109/TNNLS.2019.2919676.

[80] E. al. Ibrahim Altarawni, "Design a New Neural Network Architecture Using a Layer of Neurons," *Int. J. Recent Innov. Trends Comput. Commun.*, vol. 11, no. 9, pp. 2984–2994, 2023, doi: 10.17762/ijritcc.v11i9.9406.